

3D reconstruction of two-phase random heterogeneous material from 2D sections: An approach via genetic algorithms

D. Pizzocri^a, R. Genoni^{a,b}, F. Antonello^a, T. Barani^a, F. Cappia^{b*}

^a Politecnico di Milano, Department of Energy, Nuclear Engineering Division, Via La Masa 34, 20156, Milano, Italy.

^b Idaho National Laboratory, Characterization and Advanced PIE Division, 2525 Freemont Avenue, 83415 Idaho Falls, ID, United States.

* fabiola.cappia@inl.gov

Abstract. This paper introduces a method to reconstruct the three-dimensional (3D) microstructure of two-phase materials, e.g., porous materials such as highly irradiated nuclear fuel, from two-dimensional (2D) sections via a multi-objective optimization genetic algorithm. The optimization is based on the comparison between the reference and reconstructed 2D sections on specific target properties, i.e., 2D pore number, and mean value and standard deviation of the pore-size distribution. This represents a multi-objective fitness function subject to weaker hypotheses compared to state-of-the-art methods based on n -points correlations, allowing for a broader range of application. The effectiveness of the proposed method is demonstrated on synthetic data and compared with state-of-the-art methods adopting a fitness based on 2D correlations. The method here developed can be used as a cost-effective tool to reconstruct the pore structure in highly irradiated materials using 2D experimental data.

Keywords.

3D microstructure reconstruction; genetic algorithm; random heterogeneous material; porosity; nuclear fuel.

1. Introduction

The three-dimensional microstructure of a material participates in determining its physical properties, e.g., thermal conductivity and elastic moduli, and geometrically governs transport processes, e.g., percolation [1]. Unfortunately, the 3D microstructural features of a material are very

32 difficult to assess experimentally, with just a handful of techniques available for a limited set of
33 materials [2]. Usually, it is way easier to experimentally extract and observe 2D sections of a
34 material, and to perform measurements directly on the 2D sections of geometrical properties, e.g.,
35 phase fractions, porosity. This is particularly true for irradiated nuclear materials, for which han-
36 dling is complicated by the extreme radioactivity, which hinders the possibility to obtain 3D ex-
37 perimental data further.

38 For this reason, several methods have been developed to infer 3D material properties from 2D
39 sections, in general referred to as stereology [3]. Knowledge about the random medium to be re-
40 constructed, e.g., knowing the shape of the pores, ensures that the stereological problem has a
41 solution [4], [5]. If the type of random distribution is also known, besides few unknown parame-
42 ters, the problem is well posed. The latter is going to be the case analyzed in this work.

43 A classical methodological approach is 3D reconstruction: from a set of 2D sections, one can sta-
44 tistically represent 3D structures [6], [7]. Among the several techniques developed and applied in
45 the literature, gaussian filtering [8], [9], maximum entropy (MaxEnt) [7], and simulated annealing
46 (SA) [1], [7], [10] have proven to achieve successful 3D reconstruction results.

47 Any method applied to the reconstruction procedure must consider of the presence of local optima.
48 The complex nature of the problem and the scarce knowledge of the functional space make the
49 application of classical techniques (i.e., the Gradient Method) to solve the problem less attractive.
50 Besides the definition of the optimization function, there are several options for the optimization
51 algorithm to be used to solve the reconstruction problem. However it should be reminded that the
52 (usually) uncharted nature of the objective function—with the presence of many possible local
53 minima, large flat plains, and points where the gradient is either undefined or discontinuous—
54 makes traditional analytic techniques unfit to the task [7]. Heuristic methods are more attractive
55 since they do not depend on the characteristics of the problem, but instead leverage stochastic
56 sampling rules on deterministic decision rules [11].

57 **1.1 State-of-the-art reconstruction methods**

58 An extensive review of the available optimization algorithms applicable to 3D reconstruction is
59 out of the scope of this work (ref. [7] provides a comprehensive review). We now briefly recall
60 the main features of selected algorithms to contextualize the development of the herein proposed
61 approach.

62 Among the state-of-the-art approaches, Gaussian filtering method is at the basis of the most com-
63 monly used 3D reconstruction techniques [1]. The method uses for reconstruction only the stand-
64 ard two-point probability function for reconstruction, and employs linear and nonlinear filters on
65 Gaussian random fields (GRFs) to match the correlation function in the reconstruction process
66 [12]. However, the conventional two-point correlation is not enough to accurately characterize the
67 microstructure of the medium, and it is difficult to extend the method to include the other correla-
68 tion functions of the biphasic isotropic media [1].

69 Simulated annealing (SA) [1], [7], [10] is a heuristic reconstruction technique based on correla-
70 tions. The SA reconstruction procedure resolves to find a state of minimum *energy* among the
71 several local minima described by the target function space by swapping the phase of the voxels
72 of the digitized 3D random heterogeneous material (RHM)ⁱ [1][7]. This swapping procedure pre-
73 serves volume fractions of both phases during the reconstruction process while acting directly on
74 the connectedness of the material phases. The resulting change in the target function, ΔT , for a
75 certain swap is accepted with probability $p(\Delta T)$. This probability is evaluated via the Metropolis
76 method [1]. Acting voxel-by-voxel, SA yields a very accurate description of the reconstructed 3D
77 RHM [1], [7]. Limitations to SA are the considerable computational effort required by the ap-
78 proach when compared to, e.g., gaussian random fields and its strong dependence on the initial
79 conditions [7].

80 **1.2 Genetic algorithms applied in reconstruction methods**

81 Genetic algorithms (GA) are optimization meta-heuristic methods mimicking the biological evo-
82 lution of a population in which all the individuals are candidate solutions for a given problem [13].
83 GA differs from GRF and SA since it (1) performs a global search and (2) can be applied as Multi-
84 Objective Evolutionary Algorithms (MOEAs). MOEAs extend the capabilities of traditional evo-
85 lutionary algorithm (e.g., SA, GRF), which are usually used to solve single objective problems, by
86 the simultaneous optimization of several objectives, i.e., producing a set of non-dominated solu-
87 tions. This approach represents a novelty in the field of application, and it is advantageous for
88 being generally fit to the application of innovative optimization techniques. These features imply
89 a capability of exploring the functional space. Multi-objective GA is hence generally less prone to

ⁱ A *random heterogeneous material* (RHM) is any material composed by two or more material phases. In this work, we assume that the RHM satisfies the isotropic hypothesis. The RHM is such that the characteristic lengths of the material phases are longer than molecular lengths and shorter than the macroscopic lengths of samples [14].

90 being “trapped” into local minima compared to other methods applied to 3D reconstruction. Co-
91 herently, even if *a priori* knowledge of an approximate solution and its position in the functional
92 space can be exploited for speed-up purpose, it is not *theoretically* strictly required [13].
93 The GA uses consistently more CPU time than SA and GRF, since it invests in the exploration of
94 the solution space instead of directly converging to a minimum. GA—together with SA—has
95 proven to be the most effective method for the 3D reconstruction of multi-phase media [1], [7].
96 The goal of this work is to propose a 3D reconstruction procedure that is based on a GA and verify
97 its 3D reconstruction capabilities against synthetic 3D media that are *a priori* known. We propose
98 a 3D reconstruction approach based on an innovative definition of the target multi-objective func-
99 tion: to maintain the generality of the 3D reconstruction procedure, we do not use the correlation
100 functions as the target function, since this would impose the convergence to the correlations. The
101 correspondence of the correlations is used on the other hand for the verification of the procedure.
102 Considering the overall characteristics, we use a GA for the solution of the optimization problem.
103 After a first introduction on the definitions and hypotheses necessary for the reconstruction, the
104 frame of the GA is presented, with an description of the algorithm, the issues and limitations af-
105 fecting it, and the adopted choices to overcome them.

106

107 **2. Mathematical framework**

108 In this work, we limit our analysis to the reconstruction of 3D RHM as defined by Torquato [8].
109 We consider a RHM composed of two domains – for simplicity, we refer to one of the two domains
110 as *pores* [1]. The scale at which we define and describe RHMs is larger than the molecular scale
111 and smaller than the characteristic length of the macroscopic scale. In this way, RHM is a contin-
112 uum at the microscopic scale, whereas macroscopic or *effective* properties can be defined [14]. We
113 assume that within a RHM the domains are isotropic across the volume of the RHM itself, allowing
114 for a statistical characterization [1], [2], [7].

115 Each specific RHM can be imagined as a realization of a random process [7], [14]. Thus, a two-
116 phase RHM representing a porous medium is mathematically defined as a realization ω of a ran-
117 dom process.

118 The RHM volume $V(\omega)$ is composed of volume V_1 and volume V_2 (with $V = V_1 + V_2$), correspond-
119 ing to the two phases and defined by their respective volume fractions ϕ_1 (the *porosity*) and ϕ_2 (the

120 solid matrix). Focusing on the pore phase (identified as phase 1), we define the characteristic func-
 121 tion $I(x)$

$$I(x) = \begin{cases} 1 & \text{if } x \in V_1 \\ 0 & \text{if } x \in V_2 \end{cases} \quad (1)$$

122 where x is the position of a point in the volume V .

123 Based on the characteristic function, an RHM can be characterized by defining a set of *n-point*
 124 *correlations* [14], [15], summarizing the statistical information about the RHM itself. In this work,
 125 we use the following three correlations [6]:

- 126 • The *one-point correlation* S_1 , i.e., the probability that one random point falls within the
 127 pore phase.
- 128 • The *two-point correlation* S_2 , i.e., the probability that two random points fall within the
 129 pore phase.
- 130 • The *lineal-path correlation* S_L , i.e., the probability that one random segment falls totally
 131 within the pore phase.

132 With these definitions and under the assumption of the RHM being stationary and ergodicⁱⁱ, S_1 is
 133 independent on the position and has the same value as the pore-fraction of the medium [1], i.e.,

$$\mathbb{E}[I(x)] = S_1 = \phi_1 \quad (2)$$

134 with therefore $\phi_2 = 1 - \phi_1$ being the fraction of solid matrix. As for S_2 , it can be shown that for
 135 an isotropic RHM it depends only on the distance between the two sampled points, $|r|$, rather than
 136 on their position [1], [16], x_1 and $x_2 = x_1 + r$. Namely

$$\mathbb{E}[I(x_1)I(x_2)] = S_2(x_1, x_2) = S_2(r = x_1 - x_2) = S_2(|r|) \quad (3)$$

137 Moreover, it has two properties: (1) when distance between points tends to zero, it has the same
 138 value as ϕ_1 — i.e., the two points are coincident, and (2) when the distance tends to infinity it has
 139 value ϕ_1^2 — i.e., there is total independence of the two points. Namely

$$S_2(0) = \phi_1 \quad \text{and} \quad \lim_{r \rightarrow \infty} S_2 = \phi_1^2 \quad (4)$$

ⁱⁱ The ergodic hypothesis corresponds to the assumption that the mathematical expectations can be calculated by spatial averages on the volume V , with being V sufficiently large (practically, the minimal size of the observation volume is linked to the so-called integral range [16], [22]).

140 Lastly, S_L — which is the *lineal-path probability* — is introduced. Under the same hypothesis
 141 imposed in Eq. 3, this correlation depends only on the distance between two points, has value ϕ_1
 142 for length equal to zero, and tends to zero for infinite length. Namely

$$S_L = S_L(x, x + r) = S_L(|r|) \tag{5}$$

$$S_L(0) = \phi_1 \text{ and } \lim_{|r| \rightarrow \infty} S_L = 0 \tag{6}$$

143 This correlation contains information on the connectedness of the pore-phase of the component
 144 and is important to define the statistical limit threshold for percolation [1].

145 Under the above given ergodic assumption for an RHM and in the infinite volume limit, these
 146 correlations (Eqs. 2, 3, 5) for the 3D isotropic medium are identical to those of the 2D sections [1],
 147 [6], [14], [16]. Therefore, if the hypotheses are respected, it is possible to measure these correla-
 148 tions on the 2D sections and directly infer the respective 3D correlations [1], [6], [14]. It should
 149 be remarked that identity does not hold in general and strictly depends on the fact that the 3D RHM
 150 (and the 2D section) is isotropic and ergodic [2], [7], [14], [15]. Due to its lack of generality, the
 151 proposed 3D reconstruction technique does not enforce these identities. Nevertheless, we are going
 152 to leverage this theoretical result for the verification of the proposed 3D reconstruction technique
 153 under the above stated hypotheses [1], [7].

154 Another fundamental characteristic of an RHM is the pore-size distribution function $P(\delta)$. It is
 155 defined as the probability that a randomly sampled point in the pore phase lies at the distance
 156 between δ and $\delta + d\delta$ of the nearest point on the pore-solid interface[1].

157 The pore-size distribution and the other correlations herein defined are measurable in a virtual 3D
 158 RHM and in 2D sections (with in general no trivial correspondence between) by exploiting their
 159 probabilistic definition. A straightforward direct measuring technique is a Monte Carlo sampling
 160 of points within the RHM, followed by checking the conditions corresponding to each definition
 161 (e.g., is the sampled point within the porous phase?). Specific state-of-the-art techniques based on
 162 underlying Monte Carlo sampling have been developed and tailored for each correlation [1], [14],
 163 [15] and are adopted in this work.

164

165 **3. 3D reconstruction methodology**

166 In this section we detail the proposed 3D reconstruction technique. The main innovation brought
 167 about concerns the definition of the target multi-objective function to be minimized, whereas as

168 optimization algorithm we adopt a multi objective GA [7]. The genetic algorithm is used since it
 169 has the best features for the resolutions of complex optimization problems defined by unknown
 170 functional space [7], [11].

171 The fitness function F is a vector defined by the moments of the 2D pore-size distribution (i.e.,
 172 average size R_{2D} and standard deviation s_{2D}) and the 2D pore numberⁱⁱⁱ N_{2D} , namely

$$F = \begin{bmatrix} \sqrt{\sum_i (N_{2D,ref} - N_{2D,i})^2} \\ \sqrt{\sum_i (R_{2D,ref} - R_{2D,i})^2} \\ \sqrt{\sum_i (s_{2D,ref} - s_{2D,i})^2} \end{bmatrix} \quad (7)$$

173 where the summations over i are referred to different 2D sections extracted from a 3D RHM. Re-
 174 markably, the fitness function quantities are evaluated on the 2D sections extracted from the 3D
 175 RHM. In this way, based on the properties of the 2D section, it is possible to rank the 3D micro-
 176 structures as the most likely to produce sections that are statistically close to the reference section,
 177 and supposedly the 3D microstructures that are most likely to statistically match the original one.
 178 Furthermore, the optimization of a vector fitness function allows for simultaneous optimization of
 179 all its components, which is necessary to find the global optimum in a complex multi-objective
 180 problem such as the one treated in this work.

181 The definition of fitness provided in Eq. 7 allows overcoming hypotheses of correspondence be-
 182 tween a 3D RHM and its 2D sections, which are commonly assumed in state-of-the-art techniques
 183 [1], [2], [7], [8]. In general, these reconstruction techniques are based on the minimization of an
 184 objective function T describing the *distance* between the 2D section and the target 3D recon-
 185 structed RHM. A common formulation for T is [1]

$$T = \sum_i \alpha_i (S_{2D,ref}^{(i)} - S_{3D}^{(i)})^2 \quad (8)$$

186 where α_i are weights, and i is a symbolic index defined on the above-described correlations
 187 Eqs. 2, 3, 5). Under the hypotheses allowing to apply Eq. 8, it is formally equivalent to use $S_{2D}^{(i)}$

ⁱⁱⁱ For a stationary point process, the number of points (i.e., centers of the objects) is a random variable, and hence it would be different for different realizations and one should consider as a parameter the point density. Nevertheless, since in the following we limit our analysis to a Poisson point process with a high number of points, the discrepancy introduced is minimal.

188 instead of $S_{3D}^{(i)}$. In the following, the results obtained by using the fitness defined by Eq. 7 will be
189 systematically compared to those achievable by the state-of-the-art fitness defined by Eq. 8.

190 In this work, the ranking is based on Pareto efficiency based on simultaneous confrontation be-
191 tween the values of all three components of the fitness function in Eq. 7.

192 The proposed 3D reconstruction technique initializes a first population by randomly generating a
193 set of 3D RHMs across the space $\{N_{3D}, R_{3D}, s_{3D}\}$. Once generated, these 3D microstructures are
194 cut at a random quote generating 2D sections that are quantitatively confronted with the reference
195 2D section using the fitness function (Eq. 7). The obtained fitness value is then used to rank the
196 cubes using Pareto efficiency based on the simultaneous minimization of all the components of
197 fitness function (Eq. 7).

198 The best individuals are selected as parents and go through the variation steps to produce the off-
199 spring. Both crossover and mutation act on the 3D parameters, generating new 3D microstructures.
200 Once these are cut, their sections are confronted with the reference, and ranked together with their
201 parents, again according to Pareto efficiency as mentioned above. The environmental selection
202 saves only the fittest and kills the others for the next generation cycle. It must be stressed that, by
203 using Pareto efficiency for ranking, the algorithm yields several individuals with the same rank,
204 not a single one. This has the further advantage of preserving more effectively diversity in the
205 population and better explore the search space, preventing the search to collapse in a single result.
206 The solutions of the reconstruction procedure evolve to minimize the difference between the ref-
207 erence properties of the 2D sections and the properties of the 2D sections randomly cut from re-
208 constructed 3D media.

209 **4. Verification and validation with synthetic data**

210 As detailed in Section 3, the proposed technique for 3D RHM reconstruction is based on the min-
211 imization of the *distance* between a 2D reference image and the 2D sections of 3D reconstructed
212 RHM. The assessment strategy of the proposed 3D reconstruction technique can be conceptually
213 divided in two parts:

- 214 • The verification of the performance of the technique in localizing the minimum of the tar-
215 get function, i.e., the comparison of the 2D reference image with the 2D sections of the
216 reconstructed RHM.

- The validation of the 3D reconstruction technique itself, by comparing the 3D reference RHM (from which the 2D reference image is extracted). This validation is possible because the proposed reconstruction technique performs the optimization only based on the 2D sections, without directly forcing the characteristics of the reconstructed 3D RHM.

In this section we report the results of both these assessments for a two-phase RHM made of lognormal-distributed overlapping spherical pores. The centers of the spheres are disturbed independently, i.e., according to a Poisson point process. The resulting model is therefore a Boolean model [5], [16]. For all the assessment cases we consider synthetic data as reference, i.e., simulated 3D microstructures with known properties, as detailed below.

In principle, if the 2D statistical correlations of the simulated sections are close to the reference section, it is assumed that the correlations—hence the structure—of the simulated 3D media match those of the reference 3D medium. This has been extensively applied and verified [1], [6]–[8]; however, it is important to verify if the procedure respect this theorem. The GA must be verified independently, with convergence now achieved on the pore-size distribution.

The verification is done by applying the multi objective GA to simulated ideal reference media. If convergence on the object function of the problem yields the same 2D correlations, the 3D information of the reconstructed media is also confronted with that of the reference 3D medium. If that is verified, the GA becomes applicable to the experimental results with no *a priori* knowledge of the 3D correlations. This verification must be performed on increasingly complex microstructures, ensuring that the GA can reconstruct different experimental porous media with non-ideal features. The free parameters of the GA must also be assessed so to ensure the best efficiency of the algorithm. In this study, the free parameters of the GA are the *population size* (μ), the *selection pressure parameter* (p) for rank-based stochastic universal sampling (SUS) selection, the *crossover rate parameter*, and the *mutation rate parameter* (in this case the bitflip probability).

Population size becomes therefore crucial in defining the convergence speed [13]. An efficient population size must balance speed and accuracy of the global search. Choosing small population size eventually limits the computational cost of the GA, yet the solution will be hindered by genetic drift [17], with subsequent high risk of poor performance.

With regards to performance, selection pressure and mutation must be defined accordingly once an optimal population-size has been proposed. In presence of strong selection pressure genetic drift has little to no effect, and the population size has a weak influence, while in case of weak

248 selection pressure the population size has an heavier role in removing genetic drift [18], [19]. The
249 effect of mutation is also important and changes in relation to the population size. When the pop-
250 ulation size is large, the mutation has ill effects on the performance of the GA, while the effect is
251 beneficial if the population size is small [18].

252 Since there are few reliable theories for the determination of these parameters for better perfor-
253 mance of the GA [13], the most feasible way in our work is direct trial and error. In this work, we
254 present the solutions obtained for the best combinations of the hyperparameters of the GA applied
255 to the reconstruction of different 3D RHM.

256 The GA ability to reproduce 3D media has been applied to a pore microstructure defined by pen-
257 etrable spheres [20] whose radii follow a lognormal distribution. A lognormal distribution is de-
258 scribed by two parameters, namely 3D average radius and 3D standard deviation radius. In this
259 situation the 3D inputs are the 3D spherical pore number and the 3D lognormal distribution pa-
260 rameters. These three inputs correspond to the genes upon which the variation operators act. The
261 reference 3D microstructure is generated with the values reported in Table 1.

262 The search space for reconstruction is defined accordingly to the ranges of parameters (Table 1),
263 from which the algorithm would sample the inputs to generate the reconstructed 3D media.

264

265 Table 1. Reference value of the parameters determining the 3D RHM, together with their ranges
 266 defining the search space of the 3D reconstruction algorithm.

Parameter	Reference value	Range (search space)
3D spheres number	250,000	[200,000; 300,000]
3D average sphere radius	2.15	[2.00; 2.50]
3D standard deviation of radius	2.30	[2.00; 2.50]

267
 268 The lognormal model defines a complex structure and the presence of three genes introduces fur-
 269 ther strain on the GA. However, it is a more physical distribution than the simpler ideal case of
 270 single-sized overlapping spheres, since it represents the process of statistical realization of the
 271 multiplicative product of independent random variables [21]. Convergence to the reference data is
 272 achieved on a microstructure with porosity between 0.35 and 0.40. The hyperparameters used as
 273 settings of the GA are reported in Table 2.

274
 275 Table 2. Hyperparameters of the GA.

Hyperparameter	Value
Population size (μ)	100
Selection pressure (p)	1
Crossover rate	0.2
Mutation rate	1 / #bit

276
 277 A different mutation rate is defined for each gene of the microstructure. This way it is expected
 278 one bit-flip per each gene on average, thus maintaining diversity while avoiding ill effects of high
 279 mutation rates on convergence [18]. This, combined with a relatively low crossover rate, allowed
 280 to achieve good convergence within few tens generations of the GA. As declared before, the set of
 281 hyperparameters herein adopted is standard for the application of GA.

282 The following figures show the fitness values (Figs. 1, 3, 5) and the 2D pore-size distributions
 283 (Figs. 2, 4, 6) for the initialization, the 10th generation, and the 20th generation (at which conver-
 284 gence is achieved). The axes of Figs. 1, 3, 5 correspond to the components of the fitness function

285 F (Eq. 7), i.e., $N = \sqrt{\sum_i (N_{2D,ref} - N_{2D,i})^2}$, $R_m = \sqrt{\sum_i (R_{2D,ref} - R_{2D,i})^2}$, and $R_s = \sqrt{\sum_i (S_{2D,ref} - S_{2D,i})^2}$.

286 As it can be observed there is a wide distribution of fitness values for the whole population in the
287 initialization population (**Errore. L'origine riferimento non è stata trovata.**) that collapses dras-
288 tically towards the origin by the 10th generation (Fig. 3). By the 20th and last generation (Fig. 5),
289 the population is even more clustered around the origin, suggesting that good convergence of the
290 reconstructed media to the reference has been achieved with success. This conclusion can be de-
291 duced, albeit not as clearly, by observing the 2D pore-size distributions, as progressive conver-
292 gence of the pore-size distributions is achieved from **Errore. L'origine riferimento non è stata**
293 **trovata.**, 4, 6.
294

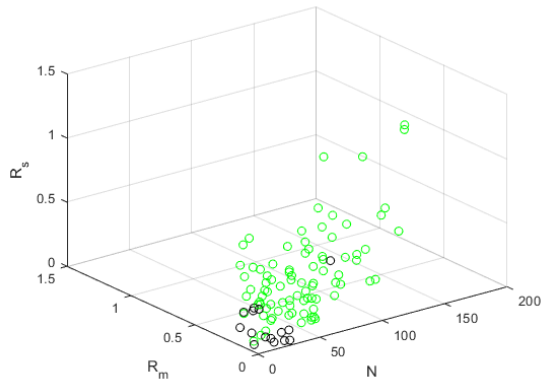


Figure 1. Fitness values of the reconstructed media (Pareto front ones in black), initialization.

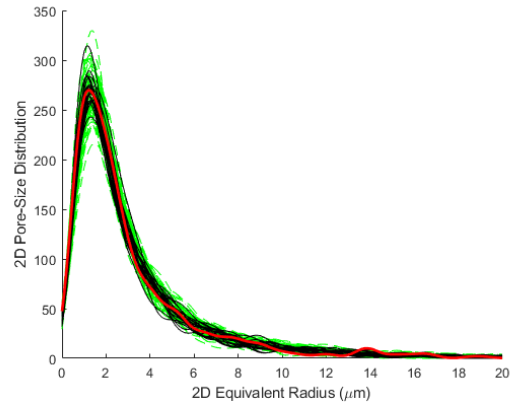


Figure 2. Pore size distribution 2D reference (red) vs. reconstructed (green) (Pareto front in black), initialization.

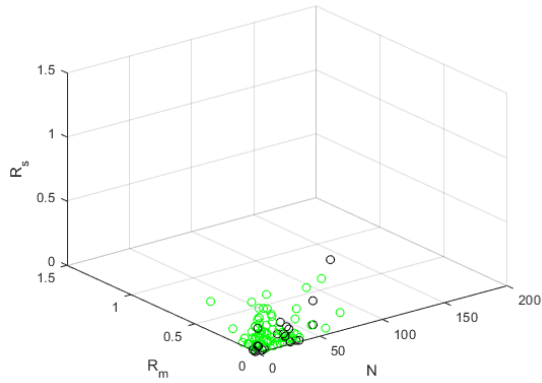


Figure 3. Fitness values of the reconstructed media (Pareto front ones in black), generation 10.

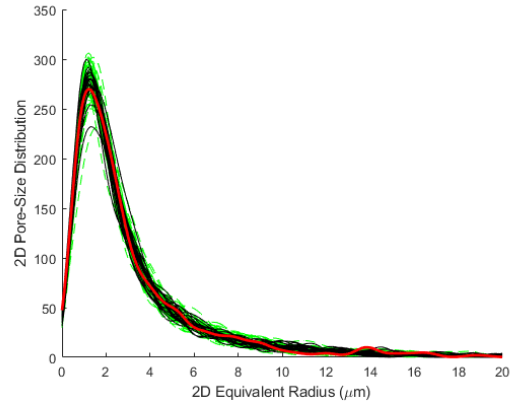


Figure 4. Pore size distribution 2D reference (red) vs. reconstructed (green) (Pareto front in black), generation 10.

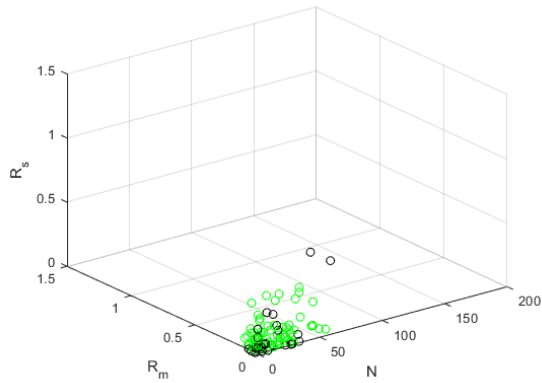


Figure 5. Fitness values of the reconstructed media (Pareto front ones in black), generation 20.

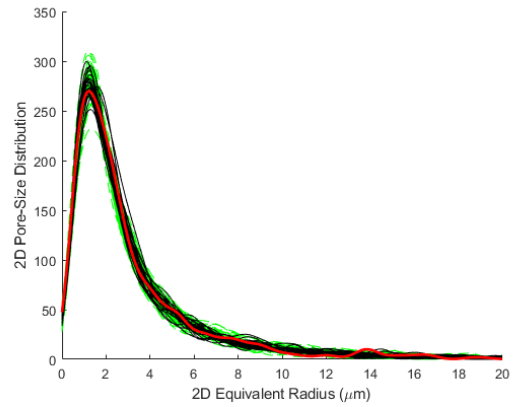


Figure 6. Pore size distribution 2D reference (red) vs. reconstructed (green) (Pareto front in black), generation 20.

295

296

297 The convergence of the fitness function also yields convergence, with a certain confidence interval,
298 to the 2D correlations of the reference section in the last generation, as shown in Fig. 7, where the
299 best individuals (on the Pareto front) of the last generation are confronted with the reference. This
300 important result verifies that the GA is able to reproduce 3D microstructures whose 2D sections
301 are statistically close to the reference image, since the correlations are the statistical descriptors of
302 the 2D pore phase [14].

303 The good results of the reconstruction procedure are noticeable from confrontation of the 2D ref-
304 erence section (extracted from the above-described 3D RHM as a midplane horizontal cross-sec-
305 tion, reported in Fig. 8) and a 2D section taken from one of the reconstructed media (Fig. 9), as
306 the statistical similarity between the two can be visibly confirmed.

307 The GA proved effective in reproducing the 2D sections of the reference medium. The most im-
308 portant verification is lastly done on the confrontation of the correlations of the 3D microstructures,
309 to verify the ability of the GA reconstruct the 3D medium. The results are satisfying since conver-
310 gence is achieved with minor deviations (Fig. 10), and the GA can reconstruct complex 3D micro-
311 structures constituted by overlapping spheres with lognormal-distributed radii.

312 For the sake of comparison, we show the results achieved by applying a state-of-the-art fitness
313 function T , as that defined by Eq. 8. Instead of targeting the convergence on the 2D pore-size
314 distribution, state-of-the-art approaches enforce the convergence on the 3D correlations. This con-
315 vergence is hence imposed on S_1 , $[\partial S_2/\partial x]_0$ (axis Lambda- S_2), and $[\partial S_L/\partial x]_0$ (axis Lambda-SL),
316 which univocally define the correlations. The comparison between Figs. 7 and 17 shows no sig-
317 nificant differences of reconstructing capabilities in terms of the 2D correlations. As for the con-
318 vergence on the pore-size distribution, by comparing Figs.1-6 to Figs. 11-16, it appears that the
319 convergence is achieved more consistently with the proposed 3D reconstruction technique^{iv}.

320

321 Validation has been performed with success on synthetic data. The ability to reproduce the refer-
322 ence cube against known cubes has been proven, and the free parameters of the GA have been
323 handled in such a way to obtain an efficient convergence to the fitness in few trials and thus in
324 shorter times despite the high computational cost of the reconstruction procedure.

325 The tests on simulated data have fitted well the data, returning a good reconstruction of the pore
326 size distribution of the 2D section of the reference media for any of the best individuals with a

^{iv} The relative difficulties in convergence could be explained considering that $[\partial S_2/\partial x]_0 \approx [\partial S_L/\partial x]_0$.

327 small variance. This also resulted in convergence to the correlations of the reference 2D section.
328 The algorithm has therefore been assessed as the convergence on the 2D pore number, and pore
329 average equivalent radius and standard deviation yields convergence to the correlations.

330 Recalling that there is correspondence between the statistical correlations of the 3D porous media
331 and the 2D section apart from small error [14], the faithful reconstruction of the sections is ex-
332 pected to yield the reconstruction of the 3D media in statistical terms. This has been demonstrated,
333 and the reconstruction has yielded good results with a certain confidence interval.

334 The proposed 3D reconstruction approach is not exempt from limitations:

- 335 • It is currently limited to application to two-phase RHMs. This could be relevant in recon-
336 structing specific nuclear materials (e.g., metallic fuel) in which one may be interested in
337 describing more phases.
- 338 • The use of a multi-objective optimization based on 2D sections allows to relax several
339 hypotheses which are usually enforced in classical stereological approaches but implies the
340 need to use heuristic algorithms to solve the problem, i.e., accepting higher computational
341 times.
- 342 • Moreover, the use of heuristic algorithms such as genetic algorithms requires considerable
343 care in the definition of the hyperparameters, implying that the proposed approach needs
344 to be tailored to specific applications.

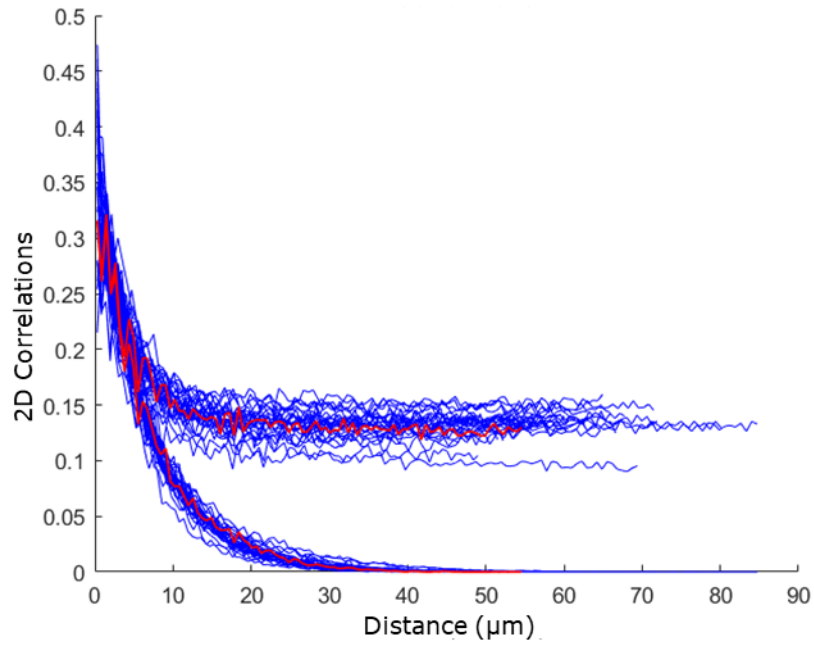


Figure 7. 2D reference correlations (S_2 curve above, S_L curve below) (red) vs. 2D reconstructed correlations from the Pareto front (blue).

345

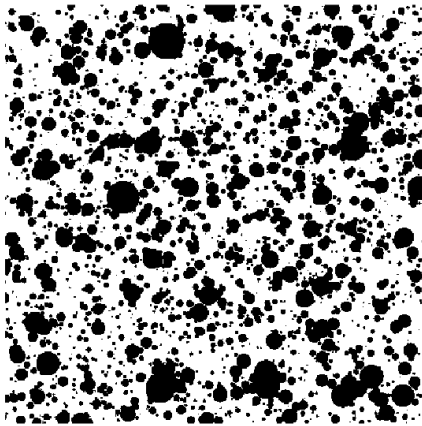


Figure 8. Example of reference 2D section.

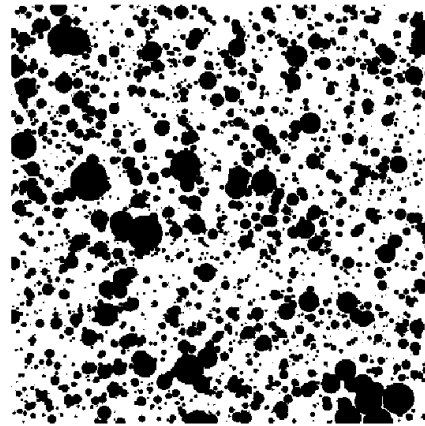


Figure 9. Example of reconstructed 2D section.

346

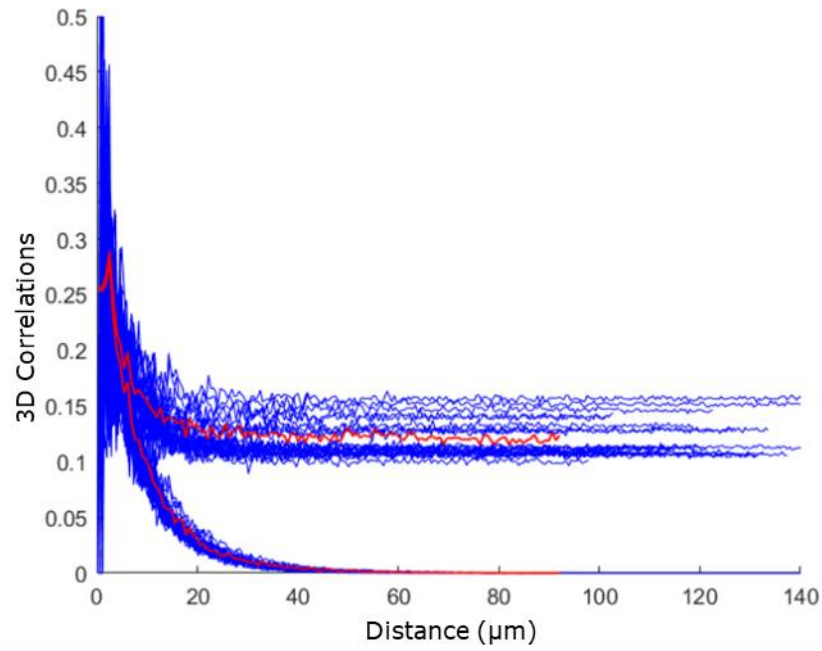


Figure 10. 3D reference correlations (S_2 curve above, S_L curve below) (red) vs. 3D reconstructed correlations from the Pareto front (blue).

347

348

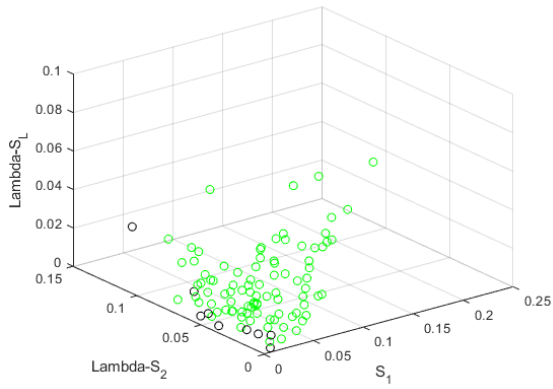


Figure 11. Fitness values of the reconstructed media (Pareto front ones in black), initialization.

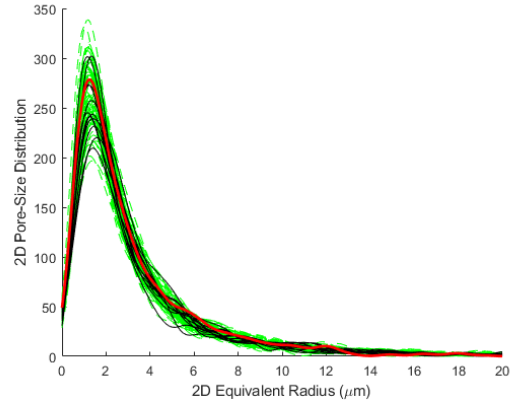


Figure 12. Pore size distribution 2D reference (red) vs. reconstructed (green) (Pareto front in black), initialization.

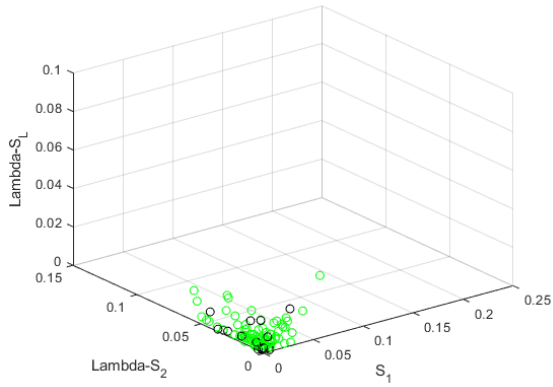


Figure 13. Fitness values of the reconstructed media (Pareto front ones in black), generation 10.

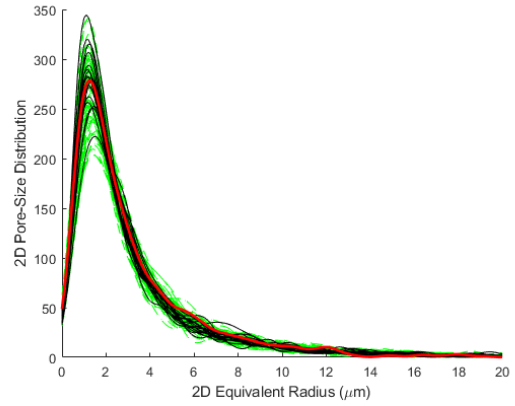


Figure 14. Pore size distribution 2D reference (red) vs. reconstructed (green) (Pareto front in black), generation 10.

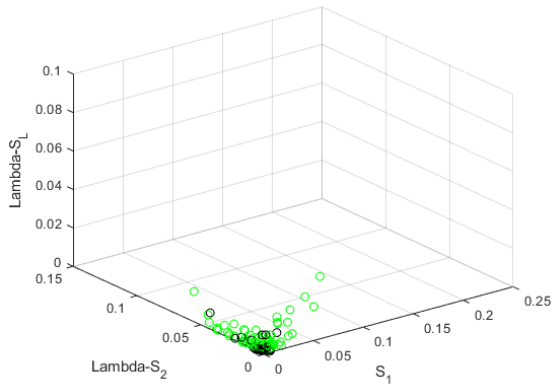


Figure 15. Fitness values of the reconstructed media (Pareto front ones in black), generation 20.

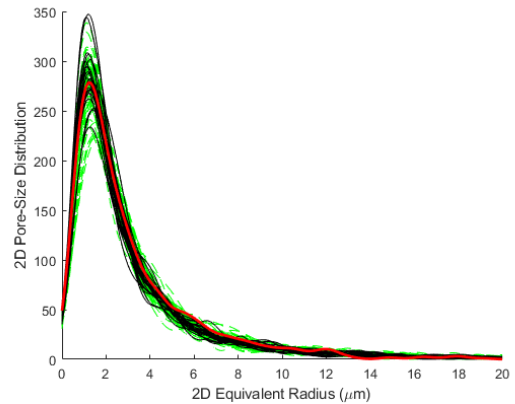


Figure 16. Pore size distribution 2D reference (red) vs. reconstructed (green) (Pareto front in black), generation 20.

349

350

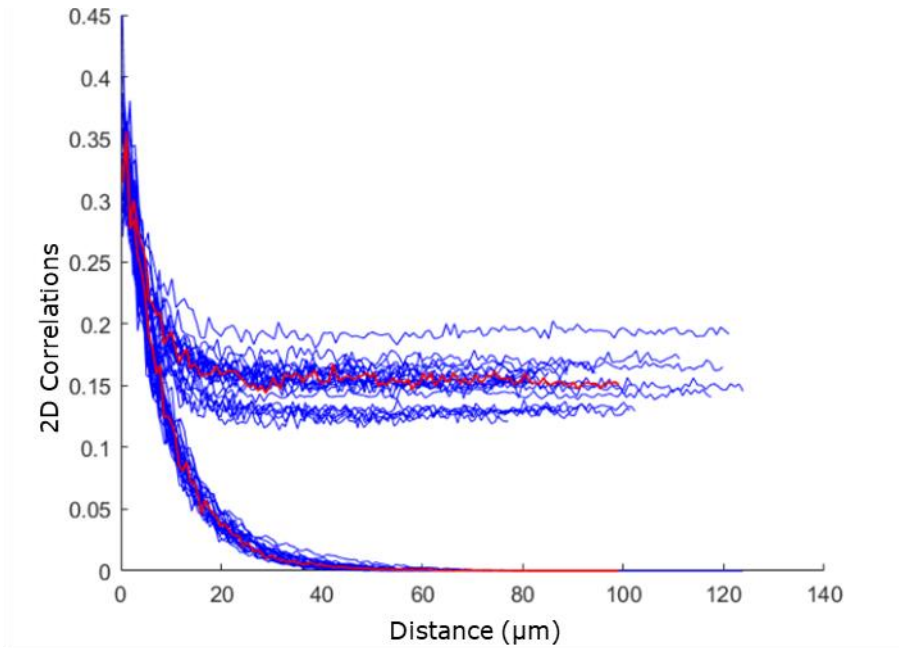


Figure 17. 2D reference correlations (S_2 curve above, S_1 curve below) (red) vs. 2D reconstructed correlations from the Pareto front (blue).

351

352

353 **5. Conclusions**

354 We have introduced a novel approach in the reconstruction of 3D RHM microstructure from the
355 limited knowledge of 2D data. The proposed approach is tailored for application to porous hetero-
356 geneous materials such as highly irradiated nuclear fuels, for which direct experimental investi-
357 gations are complex and expensive. The optimization method is based on a multi-objective opti-
358 mization genetic algorithm. Convergence is imposed between the reference and the reconstructed
359 2D sections on 2D pore number, mean value and standard deviation of the pore-size distribution.
360 This approach represents a generalization of state-of-the-art reconstruction techniques, with less
361 constraining hypotheses and thus broader applicability. Good statistical representation of the me-
362 dium is confirmed by confronting the 2D two-point correlation function and 2D lineal path func-
363 tion, from which 3D correlations can be inferred theoretically. The approach is verified and vali-
364 dated against synthetic data. Reference 3D structures with overlapping spheres whose size is log-
365 arithmically distributed, representative of highly porous materials, are reconstructed with reliable
366 confidence. The new method has been applied to the reconstruction of the pore phase in irradiated
367 fuel in a companion paper.

368

369 **Acknowledgments**

370 One of the authors would like to acknowledge financial support from the U.S. Department of En-
371 ergy (DOE), Office of Nuclear Energy under DOE Idaho Operations Office Contract DE-AC07-
372 051D14517 as part of the Nuclear Science User Facilities (NSUF), Project 17-1091.

373 The authors greatly appreciate the reviewers who have dedicated their time and expertise to this
374 manuscript.

375 **References**

- 376 [1] C. L. Y. Yeong and S. Torquato, “Reconstructing random media. II. Three-dimensional
377 media from two-dimensional cuts,” *Phys. Rev. E - Stat. Physics, Plasmas, Fluids, Relat.*
378 *Interdiscip. Top.*, vol. 58, no. 1, pp. 224–233, 1998.
- 379 [2] M. Yang, A. Nagarajan, B. Liang, and S. Soghrati, “New algorithms for virtual
380 reconstruction of heterogeneous microstructures,” *Comput. Methods Appl. Mech. Eng.*, vol.
381 338, pp. 275–298, 2018.
- 382 [3] F. Cappia *et al.*, “Critical assessment of the pore size distribution in the rim region of high
383 burnup UO₂ fuels,” *J. Nucl. Mater.*, vol. 480, 2016.

- 384 [4] D. Nychka, G. Wahba, S. Goldfarb, and T. Pugh, “Cross-Validated Spline Methods for the
385 Estimation of Three-Dimensional Tumor Size Distributions from Observations on Two-
386 Dimensional Cross Sections,” *J. Am. Stat. Assoc.*, vol. 79, no. 388, pp. 832–846, 1984.
- 387 [5] J. Serra, *Image Analysis and Mathematical Morphology*. 1983.
- 388 [6] C. L. Y. Yeong and S. Torquato, “Reconstructing Random Media,” *Phys. Rev. E*, vol. 58,
389 no. 1, pp. 224–233, 1998.
- 390 [7] E. Patelli and G. Schuëller, “On optimization techniques to reconstruct microstructures of
391 random heterogeneous media,” *Comput. Mater. Sci.*, vol. 45, no. 2, pp. 536–549, 2009.
- 392 [8] Z. Jiang, W. Chen, and C. Burkhart, “Efficient 3D porous microstructure reconstruction via
393 Gaussian random field and hybrid optimization,” *J. Microsc.*, vol. 252, no. 2, pp. 135–148,
394 2013.
- 395 [9] Y. Jiao, F. H. Stillinger, and S. Torquato, “Modeling heterogeneous materials via two-point
396 correlation functions: Basic principles,” *Phys. Rev. E - Stat. Nonlinear, Soft Matter Phys.*,
397 vol. 76, no. 3, pp. 1–15, 2007.
- 398 [10] S. Kirkpatrick, C. D. Gelatt, and M. P. Vecchi, “Optimization by Simulated Annealing,”
399 *Science (80-.)*, vol. 220, no. 4598, pp. 671–680, 1983.
- 400 [11] J. Pearl, *Heuristics: Intelligent search strategies for computer problem solving*. 1984.
- 401 [12] J. A. Quiblier, “A new three-dimensional modeling technique for studying porous media,”
402 *J. Colloid Interface Sci.*, vol. 98, no. 1, 1984.
- 403 [13] A. B. Tarek A. El-Mihoub, Adrian A. Hopgood, Lars Nolle, “Hybrid Genetic Algorithms:
404 A Review,” vol. 13, no. August, pp. 124–137, 2006.
- 405 [14] S. Torquato, *Random Heterogeneous Materials*, vol. 16. New York, NY: Springer New
406 York, 2002.
- 407 [15] S. Torquato, “Morphology and effective properties of disordered heterogeneous media,”
408 *Int. J. Solids Struct.*, vol. 35, no. 19, pp. 2385–2406, 1998.
- 409 [16] C. Lantuéjoul, *Geostatistical Simulation: Models and Algorithms*. Springer, 2002.
- 410 [17] H. Furutani, S. Katayama, M. Sakamoto, and T. Ito, “Stochastic analysis of schema
411 distribution in a multiplicative landscape,” *Artif. Life Robot.*, vol. 11, no. 1, pp. 101–104,
412 2007.
- 413 [18] Y. A. Zhang, M. Sakamoto, and H. Furutani, “Effects of population size and mutation rate
414 on results of genetic algorithm,” *Proc. - 4th Int. Conf. Nat. Comput. ICNC 2008*, vol. 1, no.

415 1, pp. 70–75, 2008.

416 [19] B. S. Weir and D. L. Hartl, “Principles of Population Genetics.,” *Biometrics*, vol. 37, no. 2,
417 p. 414, 1981.

418 [20] M. D. Rintoul and S. Torquato, “Precise determination of the critical threshold and
419 exponents in a three-dimensional continuum percolation model,” *J. Phys. A. Math. Gen.*,
420 vol. 30, no. 16, 1997.

421 [21] E. Limpert, W. A. Stahel, and M. Abbt, “Log-normal Distributions across the Sciences:
422 Keys and Clues,” *Bioscience*, vol. 51, no. 5, p. 341, 2006.

423 [22] C. Lantuéjoul, “Ergodicity and integral range,” *J. Microsc.*, vol. 161, pp. 387–403, 1991.

424